nature genetics

Muscle connective tissue controls development of the diaphragm and is a source of congenital diaphragmatic hernias

Allyson J Merrell[1], Benjamin J Ellis[2–4], Zachary D Fox[1,4], Jennifer A Lawson[1], Jeffrey A Weiss[2,3] & Gabrielle Kardon[1]

The diaphragm is an essential mammalian skeletal muscle, and defects in diaphragm development are the cause of congenital diaphragmatic hernias (CDHs), a common and often lethal birth defect. The diaphragm is derived from multiple embryonic sources, but how these give rise to the diaphragm is unknown, and, despite the identification of many CDH-associated genes, the etiology of CDH is incompletely understood. Using mouse genetics, we show that the pleuroperitoneal folds (PPFs), which are transient embryonic structures, are the source of the diaphragm's muscle connective tissue and regulate muscle development, and we show that the striking migration of PPF cells controls diaphragm morphogenesis. Furthermore, *Gata4* mosaic mutations in PPF-derived muscle connective tissue fibroblasts result in the development of localized amuscular regions that are biomechanically weaker and more compliant, leading to CDH. Thus, the PPFs and muscle connective tissue are critical for diaphragm development, and mutations in PPF-derived fibroblasts are a source of CDH.

The muscularized diaphragm is not only a unique and defining characteristic of all mammals[1] but is also an essential skeletal muscle. Diaphragm contraction drives inspiration and is critical for respiration[2]. In addition, the diaphragm has a key passive functional role, serving as a barrier between the thoracic and abdominal cavities[1]. These important functions are carried out by the costal diaphragm—a radial array of myofibers, surrounded by muscle connective tissue, that extend from the ribs to the central tendon (**Fig. 1**). Development of a functional diaphragm therefore requires the coordinated morphogenesis of muscle, muscle connective tissue and tendon, and these tissues have been suggested to develop from multiple embryonic sources[3]. However, knowledge of how this muscle develops has been limited by the inaccessibility of mammalian embryos to classic embryological experimental techniques and by a lack of genetic reagents to manipulate key embryonic sources.

Defects in diaphragm development are the cause of CDHs, which are common (1/3,000 total births) and costly (exceeding $250 million/year in the United States) birth defects[4,5]. In CDH, weaknesses in the developing diaphragm allow abdominal contents to herniate into the thoracic cavity and impede lung development. The associated lung hypoplasia is the cause of the 50% neonatal mortality and long-term morbidity associated with CDH[6]. Despite the prevalence and severity of CDH, the genetic and cellular etiology of this birth defect is incompletely understood. The majority of CDH cases appear as isolated defects[6], and the low incidence of familial recurrence suggests that CDH generally arises from *de novo* genetic mutations[7]. Molecular cytogenetic analyses of patients with CDH have identified copy number variants (CNVs) in multiple chromosomal regions strongly associated with CDH[6,8,9], and detailed analyses of these regions and a limited number of mouse studies have identified over 50 candidate CDH-causative genes[8,10]. A region that contains recurrent CDH-associated CNVs is 8p23.1 (MIM 222400)[8], and, within this region, variants in *GATA4* (encoding the GATA-binding protein 4 transcription factor) have recently been shown to strongly correlate with CDH[11–13]. Nevertheless, how these candidate CDH genes mechanistically cause CDH is not clear. Functional analyses of mouse mutants have been severely limited by early embryonic lethality[14,15], low or variable incidence of CDH[16–18] and a lack of conditional mutants[19,20]. Furthermore, the incomplete penetrance and variable expressivity of CDH-associated CNVs and genetic mutations[6,11–13] suggest that the genetic architecture underlying CDH is complex.

RESULTS

Pleuroperitoneal folds regulate diaphragm development

The diaphragm has been proposed to develop primarily from two embryonic sources. The somites are well documented to be the source of the muscle component of the diaphragm[21–23]. Less understood, the PPFs are two pyramidal-shaped mesodermal structures located between the thoracic (pleural) and abdominal (peritoneal) cavities and are hypothesized to be critical for diaphragm development[22].

[1]Department of Human Genetics, University of Utah, Salt Lake City, Utah, USA. [2]Department of Bioengineering, University of Utah, Salt Lake City, Utah, USA. [3]Scientific Computing and Imaging Institute, University of Utah, Salt Lake City, Utah, USA. [4]These authors contributed equally to this work. Correspondence should be addressed to G.K. (gkardon@genetics.utah.edu).

Received 20 October 2014; accepted 23 February 2015; published online 25 March 2015; doi:10.1038/ng.3250

However, without genetic reagents to label and manipulate the PPFs, it has been unclear what function they play in diaphragm development. A third embryonic structure, the septum transversum, has been suggested to be a source of the central tendon[22,24].

To test the contribution of the PPFs to diaphragm development and structure, we identified the first genetic reagent to label the PPFs. Given the suggestion that the PPFs are of lateral plate origin[25], we tested *Prx1-cre* (ref. 26), a transgene composed of a *Prx1* regulatory

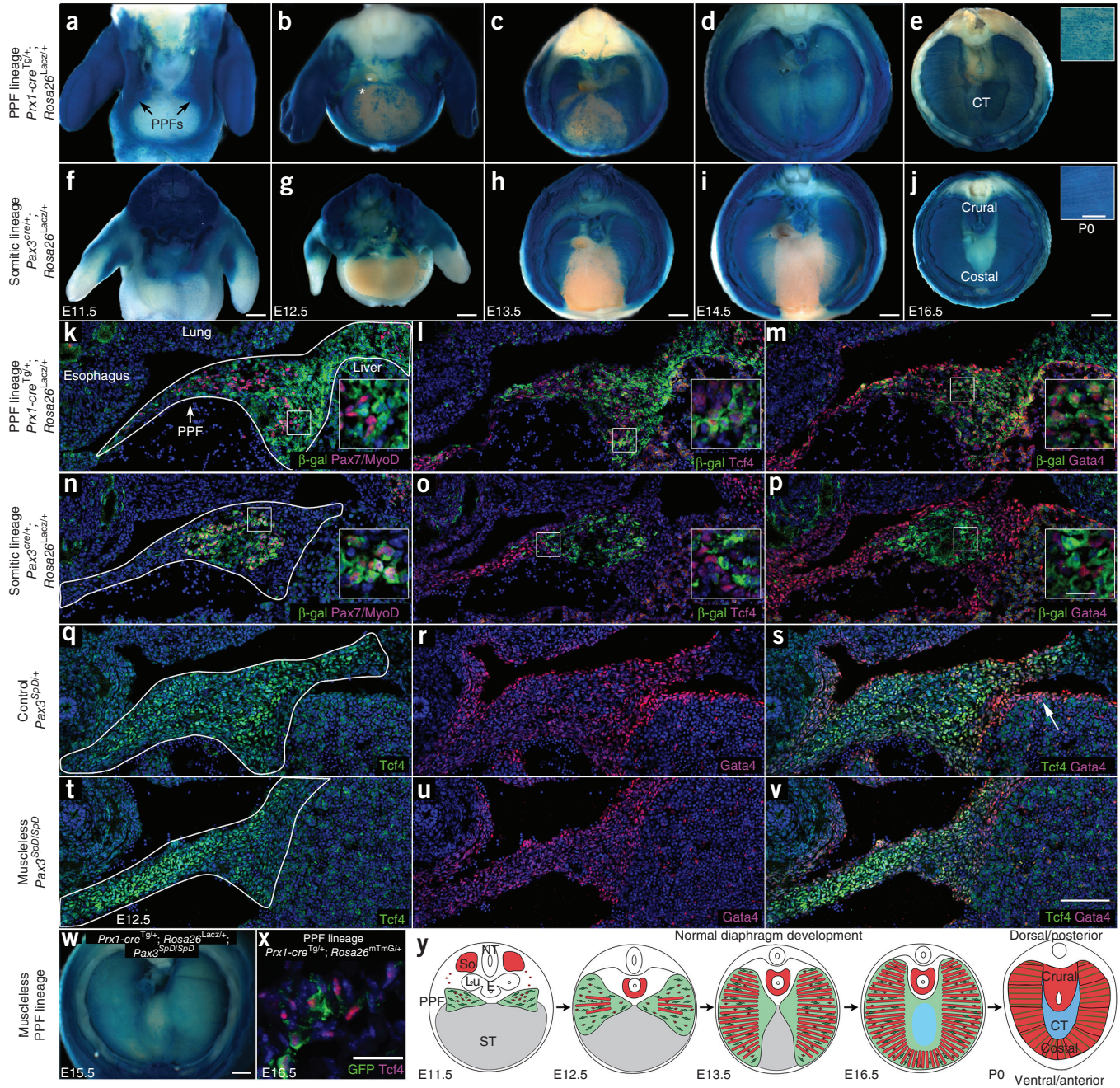

Figure 1 PPFs contain Gata4+ muscle connective tissue fibroblasts that migrate independently and in advance of myogenic cells. (**a**–**e**) The *Prx1-cre* transgene labels PPF cells (**a**) that expand throughout the diaphragm (**d**) and contribute to the central tendon (**e**) and costal muscle connective tissue fibroblasts (inset in **e**). As expected, *Prx1-cre* labels limb and body wall lateral plate mesoderm. The asterisk in **b** indicates the location corresponding Ito **Supplementary Video 1**. (**f**–**j**) *Pax3*$^{cre/+}$ labels myogenic cells (**f**) that give rise to crural and costal muscles (**j**). (**a**–**j**) Whole-mount β-galactosidase staining; $n > 5$ mice for each time point and genotype. (**k**–**m**) *Prx1-cre* does not label Pax7+ muscle progenitors or MyoD+ myoblasts (**k**) but does label Tcf4+ (**l**) and Gata4+ (**m**) fibroblasts in the PPFs. (**n**–**p**) *Pax3*$^{cre/+}$ labels Pax7+ and MyoD+ myogenic cells (**n**) but not Tcf4+ (**o**) or Gata4+ (**p**) cells. $n > 3$ mice per time point. (**q**–**v**) Gata4+ cells are Tcf4+ muscle connective tissue fibroblasts (**q**–**s**) and are present in the absence of muscle (**t**–**v**). The arrow in **s** indicates Gata4+ septum transversum. (**k**–**v**) Sections through E12.5 PPFs. (**w**,**x**) *Prx1*-derived cells expand in the absence of muscle ($n = 4/4$ embryos) (**w**) and are Tcf4+ (**x**). (**w**) Whole-mount β-galactosidase staining. (**x**) Section through E16.5 diaphragm. (**y**) Model of diaphragm development. (**a**–**j**,**w**) Dorsal at top, heart and lungs removed; (**k**–**v**) dorsal at top, medial at left. Scale bars, 250 μm (**f**), 1 mm (**j**), 100 μm (**k**–**v**), 20 μm (insets **k**–**p**), 500 μm (**g**–**i**,**w**, inset **j**), 50 μm (**x**). CT, central tendon; E, esophagus; Lu, lung; NT, neural tube; PPF, pleuroperitoneal fold; So, somite, ST,

element that drives Cre-mediated recombination in the flank and limb lateral plate mesoderm (including the limb muscle connective tissue, tendons and bones). We found that, when crossed with mice carrying the Cre-responsive reporter *Rosa26*^{LacZ} (ref. 27), mice expressing this transgene had robust labeling of the PPFs but not the septum transversum (**Fig. 1a**,**k**–**m**,**s** and data not shown). The PPFs were present at embryonic day (E) 11.5 and expanded across the surface of the liver to give rise to cells throughout the diaphragm at E14.5 (**Fig. 1a**–**d**). Although mice carrying *Prx1-cre* labeled body wall non-muscle tissues (**Fig. 1a**–**e**), these cells did not appear to contribute to the diaphragm (as determined by two-photon studies). PPF cells were distinct from somite-derived muscle progenitors, myoblasts and myofibers (**Fig. 1e**,**k**). Instead, the PPFs gave rise to two non-myogenic tissues. First, in contrast to the previous hypothesis that the central tendon derives from the septum transversum[22,24], the PPFs gave rise to the central tendon (**Fig. 1e**). Second, the PPFs gave rise to muscle connective tissue fibroblasts. *Prx1*-derived cells (cells genetically labeled by *Prx1-cre*) expressed the muscle connective tissue marker Tcf4 (also known as Tcf7l2)[28,29] in E12.5 PPF (**Fig. 1l**) and in the fully developed diaphragm (**Fig. 1x**), and these cells ultimately resided interstitial to costal (but not crural) myofibers (**Fig. 1e**). Notably, PPF cells also strongly expressed the product of the CDH-implicated gene *Gata4*; at E12.5, most *Prx1*-derived cells expressed Gata4 (**Fig. 1m**), and all Tcf4$^+$ fibroblasts were Gata4$^+$ (**Fig. 1q**–**s**). Thus, we demonstrate that the PPFs are not simply transient developmental structures but ultimately give rise to the central tendon and the muscle connective tissue fibroblasts (**Fig. 1y**). Furthermore, the expression in PPF cells of CDH-implicated Gata4 (as also noted previously[12,16,30]) suggests that the PPFs might be important in the etiology of CDH.

To trace the contribution of myogenic cells to diaphragm morphogenesis and determine their spatiotemporal relationship to PPF cells, we genetically labeled myogenic cells using *Pax3*$^{cre/+}$; *Rosa26*$^{LacZ/+}$ mice[31], in which Cre-mediated recombination in the somite labels all myogenic cells. Myogenic cells migrated from the somite and entered the PPFs by E11.5 (**Fig. 1f**,**n**), then spread ventrally and dorsally (**Fig. 1g**–**i**), differentiated into myofibers (**Fig. 1h**,**i**) and formed a completely muscularized diaphragm by E16.5 (**Fig. 1j**). Comparison of muscle and PPF morphogenesis showed that the PPFs expanded ventrally in advance of the muscle (**Fig. 1d**,**i**). Labeled myogenic cells did not express either Tcf4 or Gata4 but instead were surrounded by non-myogenic Tcf4$^+$Gata4$^+$ cells (**Fig. 1o**,**p**). The migration of myogenic cells into the PPFs and their subsequent expansion within but behind the leading edge of PPF cells suggest that the PPFs might guide the morphogenesis of the diaphragmatic muscle (**Fig. 1y**).

If the PPFs are critical for regulating the morphogenesis of the diaphragm's muscle, we would expect the formation and morphogenesis of the PPFs to occur independently of that of muscle. To test this hypothesis, we analyzed *Prx1-cre*$^{Tg/+}$; *Rosa26*$^{LacZ/+}$; *Pax3*$^{SpD/SpD}$

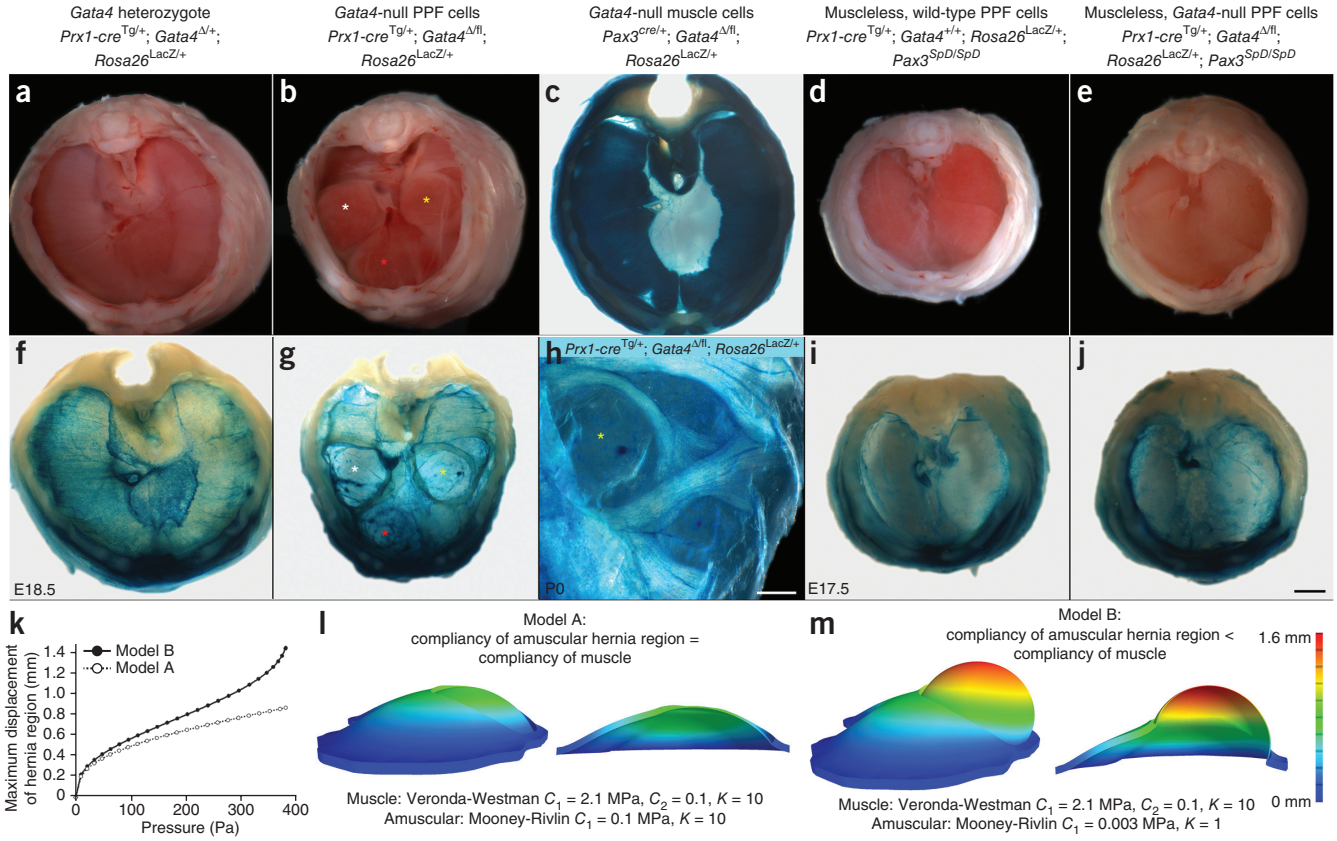

Figure 2 Deletion of *Gata4* in the PPFs produces localized amuscular regions that are weaker than juxtaposed muscular regions and results in CDH. (**a**–**d**) CDH develops in mice with *Gata4*-null PPF cells ($n > 33/33$; Bochdalek hernias are labeled with white and yellow asterisks, and a Morgagni hernia is labeled with a red asterisk) (**b**) but not in mice heterozygous for *Gata4* loss ($n > 66/66$) (**a**), mice with *Gata4*-null muscle ($n = 28/28$) (**c**) or mice with muscleless diaphragms ($n > 10/10$) (**d**). (**e**,**j**) Loss of muscle in diaphragms with *Gata4*-null PPF cells rescues herniation, indicating that juxtaposition of amuscular with muscular regions is required for CDH ($n = 3/3$ mice). (**f**,**i**) In mice heterozygous for *Gata4* loss (**f**) or lacking muscle (**i**), PPF cells are present in the diaphragm. (**g**,**h**) In herniated regions, PPF cells are present, but muscle is not ($n = 7/7$ mice). (**k**–**m**) Finite element modeling shows that a hernia only develops when the amuscular region is more compliant than the muscular region. Models are lateral views. (**c**,**f**–**j**) Whole-mount β-galactosidase staining. (**a**–**j**) Dorsal is at top. Scale bars, 1 mm (**a**–**g**,**i**,**j**), 0.5 mm (**h**).

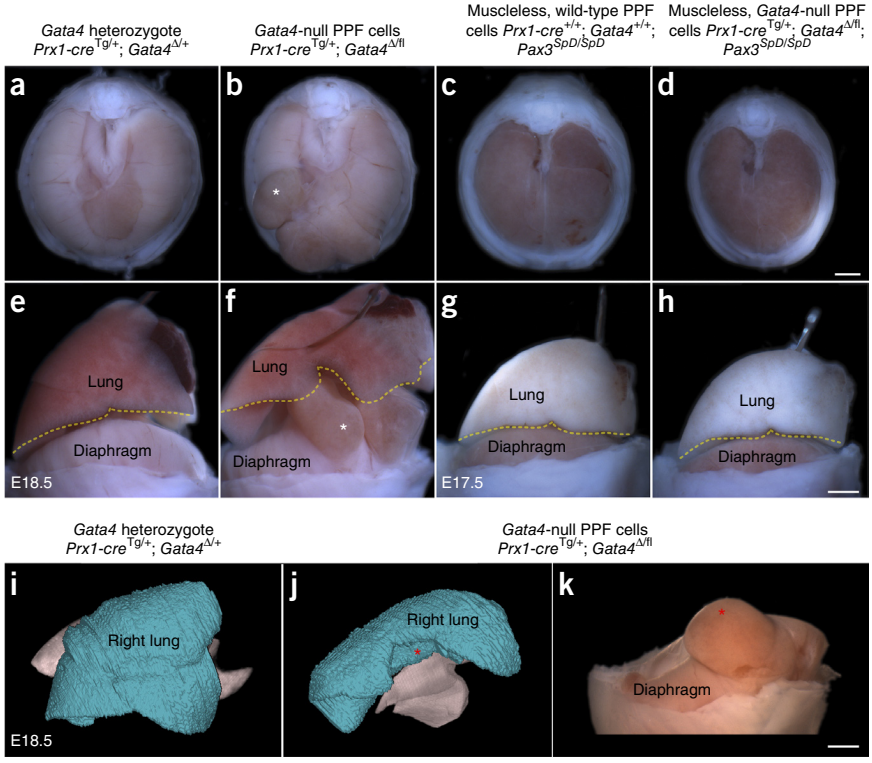

Figure 3 In CDH, physical impedance by herniated tissue causes lung hypoplasia. (**a**,**b**,**e**,**f**) As compared with lungs in mice with a normal diaphragm ($n > 50$) (**a**,**e**), development of lung lobar structure is impeded by liver herniated through a defective diaphragm ($n = 8/8$; white asterisks indicate the equivalent herniated region in **b** and **f**). (**c**,**d**,**g**,**h**) Lungs develop normally in mice with a muscleless diaphragm ($n > 5/5$) (**c**,**g**) or with a muscleless diaphragm with *Gata4*-null PPF cells ($n = 2/2$) (**d**,**h**). Yellow lines outline the surface of lungs adjacent to the diaphragm. (**i**–**k**) MicroCT scans show that lung size (**i**,**j**) is greatly reduced in the presence of hernia ($n = 3$; red asterisks indicate the equivalent herniated region in **j** and **k**). (**i**,**j**) Lateral right view of lungs, with right lungs shown in blue; (**k**) lateral view of a diaphragmatic hernia associated with malformed lungs (**j**). (**a**,**b**,**e**,**f**,**i**–**k**) E18.5; (**c**,**d**,**g**,**h**) E17.5. Scale bars, 1 mm (**a**–**d**), 1 mm (**e**–**h**,**k**).

mice[32] (the SpD allele contains a point mutation that prevents the emigration of muscle progenitors from the somites), which have a muscleless diaphragm. We found that, indeed, even in the absence of muscle, PPF cells were present and expressed Tcf4 and Gata4 (**Fig. 1t**–**v**) at E12.5 and subsequently underwent normal morphogenetic expansion (**Fig. 1w**).

The expansion of PPF cells, even in the absence of muscle, suggests that the morphogenetic movement of PPF cells drives normal diaphragm morphogenesis. Although static images of PPF cells suggest that these cells migrate across the surface of the liver, it is formally possible that this pattern simply reflects the dynamic activation of *Prx1-cre* and not cell movement. To test this, we cultured *ex vivo* E12.5 diaphragms (with the ribs and underlying liver intact) and imaged genetically labeled PPF cells via two-photon microscopy. We found that PPF cells actively migrated across the liver surface (at the rate of 5 μm/h); although a few cells migrated singly, most appeared to migrate collectively (**Fig. 1b**, **Supplementary Fig. 1** and **Supplementary Videos 1** and **2**). This collective PPF cell migration, which occurred independently of muscle, likely drives diaphragm morphogenesis.

CDH originates with defects in PPF-derived fibroblasts

Human genetic studies have shown that noncoding variants and missense mutations of *GATA4* are correlated with CDH[11–13], but explicit tests of the function of *Gata4* in the development of CDH have been limited by the early embryonic lethality of *Gata4*-null mice[14,15] and the reported low penetrance of CDH in mice with heterozygous loss of *Gata4* (ref. 16). The strong Gata4 expression in the PPFs (**Fig. 1**)[12,16,30] suggests that Gata4 functions in this tissue. To test this hypothesis, we generated *Prx1-cre*$^{Tg/+}$; *Gata4*$^{\Delta/fl}$ mice (using *Gata4*^{fl} mice[33]), in which one allele (Δ) of *Gata4* is deleted in the germ line and the other allele (floxed, fl) is deleted specifically in the PPFs (**Fig. 2**). Strikingly, we found that 100% of mutant mice ($n > 33/33$) developed multiple hernias throughout the diaphragm (**Fig. 2a**,**b**). Similar to patients with CDH[6,34], in *Prx1-cre*$^{Tg/+}$; *Gata4*$^{\Delta/fl}$ mice, the size and location of hernias varied: most (68%) formed in the dorsal lateral diaphragm (Bochdalek hernias), and the rest (32%) developed in the ventral diaphragm (Morgagni hernias; **Fig. 2b**). We found that hernias only occurred in muscle-associated regions and not in the central tendon. Thus, although the PPFs give rise to both the muscle connective tissue and the central tendon, hernias never arise in the central tendon, and it is thus defects in the PPF-derived muscle connective tissue that cause CDH in these mice. Unlike previous reports[16], we never observed diaphragm defects in heterozygous *Gata4*$^{\Delta/+}$ mice ($n > 66/66$; **Fig. 2a**). In addition, we tested whether *Gata4* was required in myogenic cells for diaphragm development by analyzing *Pax3*$^{cre/+}$; *Gata4*$^{\Delta/fl}$ mice. As predicted given the lack of Gata4 expression in myogenic cells, diaphragms developed normally in these mice ($n = 28/28$; **Fig. 2c**). Because *Pax3* is also expressed in neural crest cells, this experiment rules out neural crest as a source of CDH from *Gata4* mutations. Thus, we definitively demonstrate that *Gata4* null mutations cause CDH. Moreover, defects in the PPFs and muscle connective tissue are a source of CDH.

Localized weaker amuscular regions give rise to hernias

Our results demonstrate that, with complete penetrance, loss of *Gata4* in PPF-derived muscle connective tissue fibroblasts results in diaphragmatic hernias, but what mechanistically causes herniation? The most commonly proposed mechanism is that hernias are caused by a morphogenetic defect in the PPFs; this defect results in a localized loss of PPF-derived tissue, a consequent absence of the muscle normally associated with this tissue, formation of a hole in the diaphragm and herniation of growing abdominal tissue through this hole[24,35]. If this hypothesis is true, PPF-derived cells and associated muscle should not be present in herniated regions. To test this, we examined *Prx1-cre*$^{Tg/+}$; *Gata4*$^{\Delta/fl}$; *Rosa26*$^{LacZ/+}$ mice, in which PPF-derived *Gata4*-null fibroblasts are positive for β-galactosidase (β-gal$^+$) and muscle is β-gal$^-$. Surprisingly, β-gal$^+$ fibroblasts were present as a sac covering the herniated regions, and these regions were thus not simply holes in this tissue ($n = 7/7$; **Fig. 2g**,**h**). Yet, the sacs were devoid of muscle, and the muscle surrounding the sacs was aberrantly patterned (**Fig. 2g**,**h**). Therefore, although muscle is absent in herniated regions, hernias in *Prx1-cre*$^{Tg/+}$; *Gata4*$^{\Delta/fl}$ mice are not caused by a failure of the morphogenetic expansion of the PPFs and the formation of holes in the diaphragm.

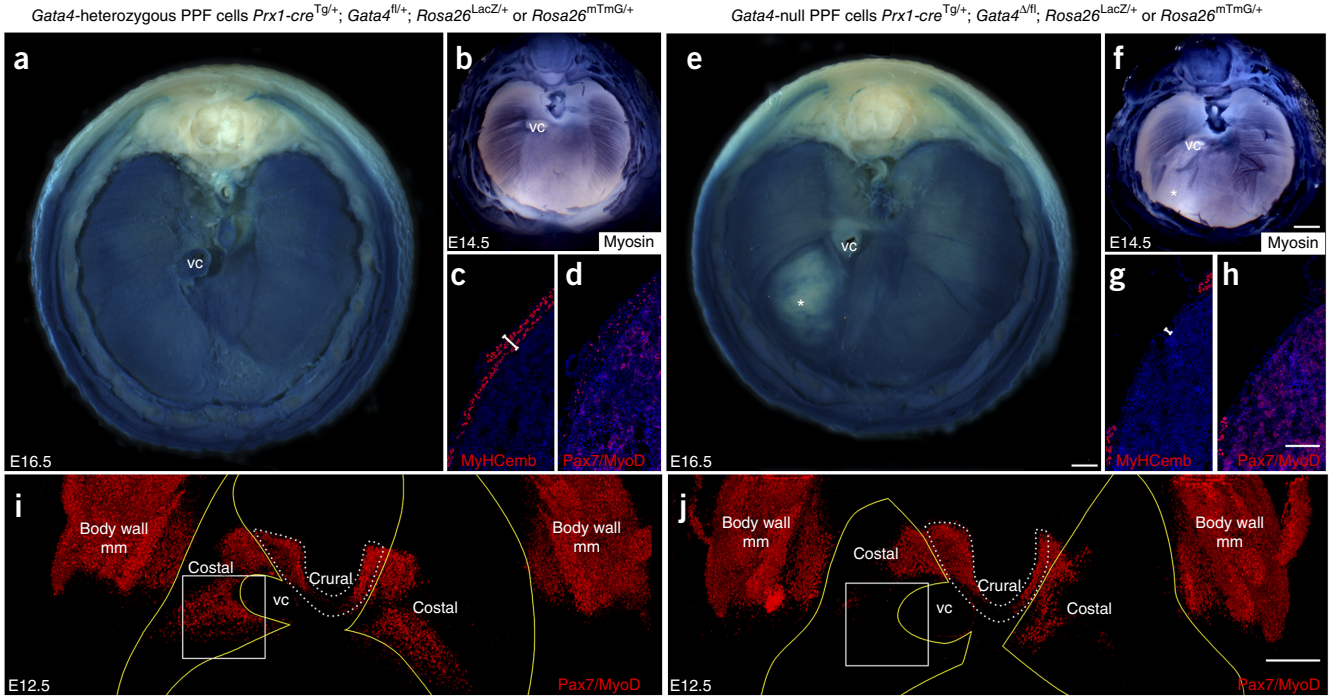

Figure 4 CDH results from early defects in the localization of muscle progenitors. (**a**,**e**) Overt liver herniation through diaphragms with *Gata4*-null PPF cells first appears at E16.5 (asterisk in **e**; $n = 3/3$ mice). (**b**–**d**,**f**–**h**) At E14.5, differentiating myofibers are aberrant (asterisk in **f**; $n = 7/7$ mice) (**b**,**f**), and myofibers (**c**,**g**) and Pax7$^+$ and MyoD$^+$ muscle progenitors (**d**,**h**) are absent in localized regions ($n = 1/1$ mouse). (**a**,**b**) Whole-mount β-galactosidase staining; (**b**,**f**) whole-mount myosin–alkaline phosphatase staining; (**c**,**d**,**g**,**h**) section immunofluorescence. (**i**,**j**) At E12.5, Pax7$^+$ and MyoD$^+$ muscle progenitors are absent in localized regions, particularly in the region (box) that consistently gives rise to hernias ($n = 7/7$ mice). The PPFs are outlined in yellow (outline derived from the GFP immunofluorescence shown in **Fig. 6a**,**b**), and crural muscle is outlined in white dotted lines. Whole-mount immunofluorescence (the same diaphragms are shown in **Fig. 6a**,**b**). (**a**,**b**,**e**,**f**,**i**,**j**) Dorsal is at the top. Scale bars, 500 μm (**a**,**e**), 500 μm (**b**,**f**), 100 μm (**c**,**d**,**g**,**h**), 200 μm (**i**,**j**). VC, vena cava; body wall mm, body wall muscles.

A second hypothesis for how CDH develops is that PPF-derived muscle connective tissue alone, without muscle, is weak and allows herniation through the weaker tissue. We tested this hypothesis by examining *Prx1-cre*$^{Tg/+}$; *Rosa26*$^{LacZ/+}$; *Pax3*$^{SpD/SpD}$ diaphragms, in which muscle is absent but PPF-derived muscle connective tissue is present (**Fig. 1w**). However hernias never formed in these mice with muscleless diaphragms ($n > 10/10$; **Fig. 2d**,**i**). This demonstrates that PPF-derived muscle connective tissue alone, even in the absence of muscle, is sufficiently strong to prevent herniation of abdominal tissues.

These data suggest two additional hypotheses for the mechanism underlying herniation. First, the muscle connective tissue produced by *Gata4*-null fibroblasts may be weaker than the connective tissue generated from wild-type fibroblasts, and this weaker tissue might allow for herniation of abdominal tissue. Alternatively, formation of relatively weak regions of amuscular connective tissue juxtaposed to stronger, muscularized regions might allow abdominal contents to herniate through the localized weak regions. To test these possibilities, we generated *Prx1-cre*$^{Tg/+}$; *Gata4*$^{\Delta/fl}$; *Pax3*$^{SpD/SpD}$ mice, in which diaphragms are muscleless and the PPF-derived fibroblasts are *Gata4* null. If the first hypothesis is correct, then hernias should form, whereas, if the second hypothesis is correct, hernias should be absent. Strikingly, no hernias developed in these mice ($n = 3/3$), and the diaphragms were indistinguishable from those of *Pax3*$^{SpD/SpD}$ mice (**Fig. 2d**,**e**,**i**,**j**). Thus, loss of muscle rescues the herniation phenotype of *Prx1-Cre*$^{Tg/+}$; *Gata4*$^{\Delta/fl}$ mice. This demonstrates that the muscle connective tissue produced by *Gata4*-null fibroblasts is not inherently weaker than wild-type connective tissue. Instead, hernias

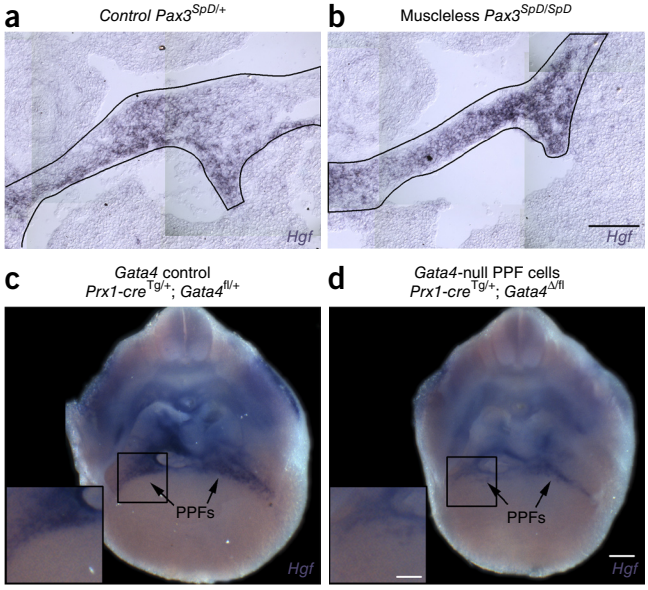

Figure 5 *Hgf* is strongly expressed in PPF cells and downregulated in *Gata4*-null fibroblasts. (**a**–**c**) *Hgf* is expressed in PPF cells independently of muscle. PPFs are outlined in black. (**d**) Deletion of *Gata4* in PPF cells leads to *Hgf* downregulation, particularly in the region (box) that consistently gives rise to hernias ($n = 11/11$ mice). Dorsal is at the top of all panels. Scale bars, 100 μm (**a**,**b**), 250 μm (**c**,**d**), 125 μm (insets in **c**,**d**).

only develop when localized regions of amuscular connective tissue develop in juxtaposition with muscularized regions; abdominal tissue herniates through these amuscular regions that are relatively weaker than muscularized regions.

To gain further insight into the biomechanics governing herniation, we turned to finite element modeling. The amuscular regions of E14.5 diaphragms, before overt herniation of abdominal tissue, were 25% of the thickness of the muscular regions. This suggests that the relative weakness of the amuscular regions in comparison to the muscular regions could simply be due to their decreased thickness. Alternatively, the amuscular regions might be both thinner and composed of a more compliant material than muscle. We tested this possibility by creating a finite element model. The geometry of the diaphragm was based on the dimensions of an E16.5 mutant diaphragm, and a uniform, physiologically reasonable pressure was applied to the diaphragm to simulate the pressure of the growing liver. Using the FEBio nonlinear finite element solver[36], when the muscle material behavior was represented by an isotropic hyperelastic constitutive equation[37] and the amuscular region was made substantially more compliant (deforms more in response to an applied force) than the muscle, a pressure of 380 Pa induced a bulge in the amuscular region that matched the geometry of the hernias in experimental mice (model B; **Fig. 2k**,**m** and **Supplementary Videos 3** and **4**). In contrast, when the thinner amuscular region was assigned the same material properties as the

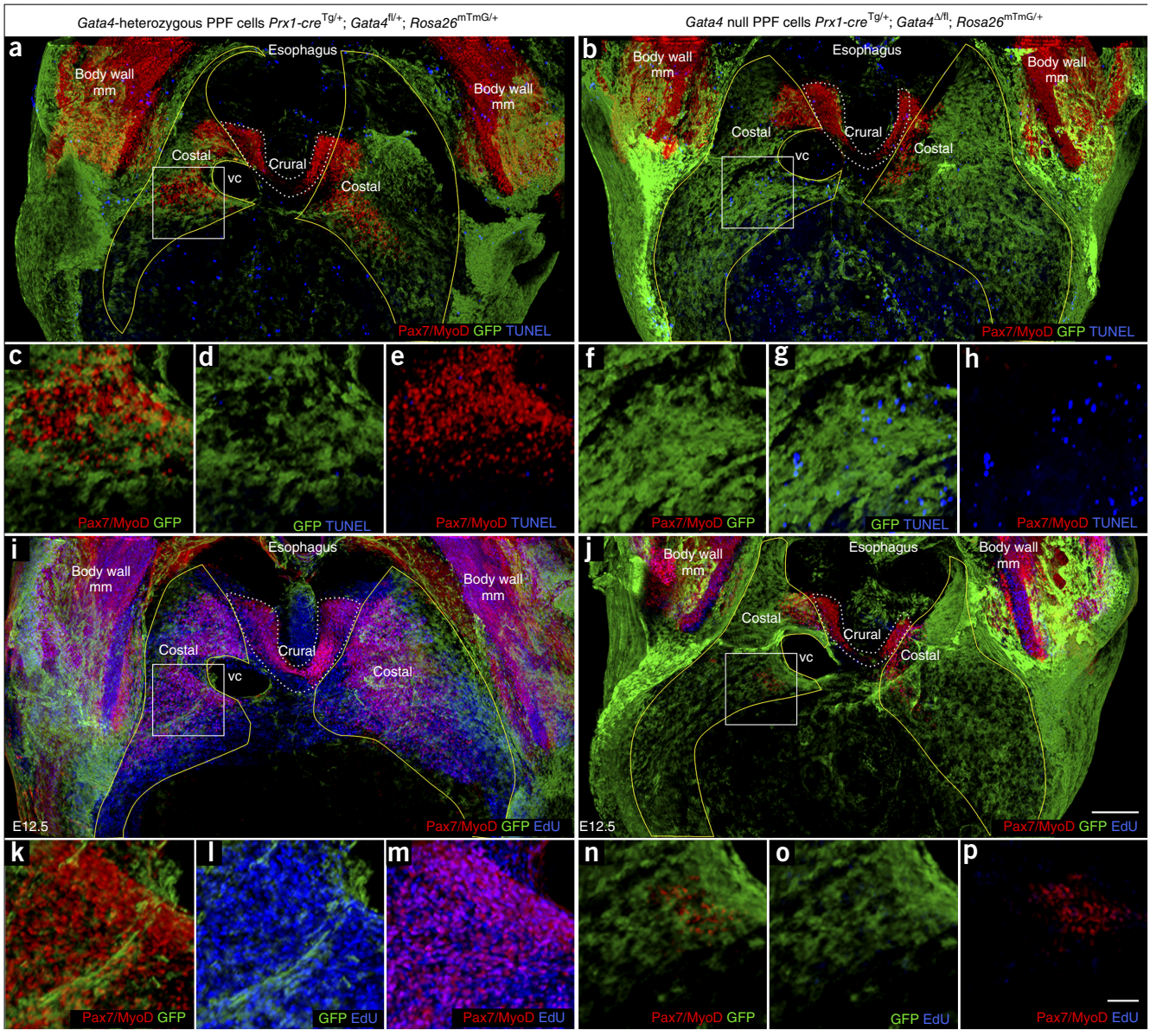

Figure 6 Early defects in proliferation, apoptosis and localization of muscle progenitors lead to CDH. (**a**–**h**) At E12.5, there is a marked increase in the number of apoptotic cells in diaphragms with *Gata4*-null PPF cells (**b**,**f**–**h** versus **a**,**c**–**e**), particularly in the region (boxes in **a** and **b**, magnified in **c**–**e** and **f**–**h**, respectively) that consistently give rise to hernias (n = 3/3 mice). (**i**–**p**) There is also a marked decrease in the number of EdU$^+$ proliferating cells in mutant diaphragms (n = 7/7 mice) (**j**,**n**–**p** versus **i**,**k**–**m**). In the region (boxes in **i** and **j**, magnified in **k**–**m** and **n**–**p**, respectively) destined to give rise to hernias, the few myogenic cells are EdU$^-$. (**a**–**p**) Costal muscle progenitors are surrounded by GFP$^+$ PPF cells in control diaphragms but are excluded from regions with GFP$^+$ *Gata4*-null PPF cells in mutant diaphragms, particularly in regions destined to form hernias (boxes in **b** and **j**, magnified in **f**–**h** and **n**–**p**, respectively). (**a**–**p**) Whole-mount immunofluorescence. (**a**,**b**,**i**,**j**) PPFs are outlined in yellow, and costal muscle is outlined in white dashed lines. Dorsal is at the top for all panels. Scale bars, 200 μm (**a**,**b**,**i**,**j**), 50 μm (**c**–**h**,**k**–**p**). VC, vena cava; body wall mm, body wall muscles.

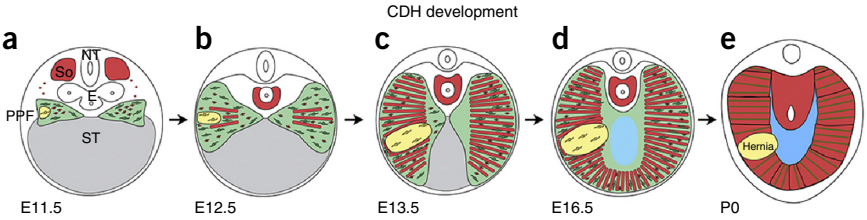

Figure 7 Model of CDH development. Our data support a model whereby CDH arises from early genetic mutations in a subset of PPF-derived muscle connective tissue fibroblasts (**a**; mutant fibroblasts are yellow, wild-type fibroblasts are green). Mutant fibroblasts clonally expand and inhibit muscle progenitors from developing in these regions (via decreased proliferation and increased apoptosis of muscle progenitors), resulting in local regions (shown in yellow) that are amuscular but contain connective tissue fibroblasts and their associated extracellular matrix (**b**–**d**). Amuscular regions are thinner and more compliant than surrounding thicker and stiffer muscularized diaphragm and allow herniation of abdominal contents into the thoracic cavity (**d**,**e**). PPF, pleuroperitoneal fold; NT, neural tube; So, somite; ST, septum transversum; VC, vena cava.

muscle, pressures up to 380 Pa were unable to generate a bulge in the amuscular region (model A; **Fig. 2k**,**l**). Together, these results indicate that the weakness in the amuscular regions is due to both their decreased thickness and increased compliance as compared with the muscularized regions.

Herniated tissue physically impedes lung development

The neonatal mortality and long-term morbidity of patients with CDH are caused by secondary lung hypoplasia, which is thought to arise from the physical impedance of lung growth by herniated abdominal tissue. However, a 'dual-hit' hypothesis has also been proposed[38], whereby lung hypoplasia can result both from physical impedance by herniated tissue and cell-autonomous effects on lung development by CDH-associated genes. Consistent with this hypothesis, mutations in *Gata4* can affect lung development in a cell-autonomous manner[39]. Similar to patients with CDH, *Prx1-cre*$^{Tg/+}$; *Gata4*$^{\Delta/fl}$ mice had low O_2 blood saturation (as measured by pulse oximetry; data not shown), and most died within a few hours of birth. We found defects in the lung lobar structure in all mice examined (n = 8/8; **Fig. 3**), and these defects resulted in up to a 34% reduction in lung volume (as quantified from microCT scans) of lobes adjacent to hernias (**Fig. 3i**–**k** and **Supplementary Videos 5** and **6**). The tight correlation of lung defects with hernias in all mice examined strongly suggests that herniated tissue physically impedes lung growth in these mice. Furthermore, the absence of lung defects in *Prx1-cre*$^{Tg/+}$; *Gata4*$^{\Delta/fl}$; *Pax3*$^{SpD/SpD}$ mice (**Fig. 3c**,**d**,**g**,**h**) argues that herniation precedes and causes lung hypoplasia. Thus, *Prx1-cre*$^{Tg/+}$; *Gata4*$^{\Delta/fl}$ mice not only develop CDH but also the lung defects and neonatal lethality typically accompanying CDH, and impedance of lung growth by herniated tissue is sufficient to induce lung lobar defects. It is also likely that *Gata4* mutations have additional cell-autonomous effects on lung development (as shown in ref. 39), although we could not directly evaluate this, as *Prx1-cre* has low levels of recombination in the lungs, and the alveolar structure was largely unaffected in these mutant mice (**Supplementary Fig. 2**).

Aberrant HGF levels and muscle proliferation and apoptosis in CDH

Our experiments demonstrate that hernias form when localized amuscular regions develop within the muscular diaphragm. To determine when hernias and amuscular regions arise, we examined a developmental time series of mutant *Prx1-cre*$^{Tg/+}$; *Gata4*$^{\Delta/fl}$ embryos (**Fig. 4**). Overt herniation of liver through the diaphragm first occurred at E16.5 (**Fig. 4a**,**e**). However, defects in muscle were present by E14.5 (**Fig. 4b**,**f**), and neither differentiated myofibers nor muscle progenitors were present in amuscular regions (**Fig. 4c**,**d**,**g**,**h**). Even at E12.5, there was a profound defect in the number and localization of muscle progenitors (**Fig. 4i**,**j**).

A critical early regulator of the muscle progenitors migrating into the limb and diaphragm, and therefore an attractive candidate downstream target of Gata4, is hepatocyte growth factor (HGF)[23,40,41]. We found in control mice that PPF cells, independently of the presence of muscle, robustly expressed *Hgf* at E12–E13.5 (**Fig. 5a**–**c**), whereas muscle progenitors expressed the HGF receptor *Met* (data not shown). In *Prx1-cre*$^{Tg/+}$; *Gata4*$^{\Delta/fl}$ E12.5 diaphragms, *Hgf* levels were markedly downregulated and diminished in regions that consistently give rise to hernias (n = 11/11; **Fig. 5d**).

Because HGF functions as a mitogen and a cell survival factor[42], we examined whether changes in apoptosis and proliferation determine why fewer muscle progenitors are present in mutant embryos (**Fig. 6** and **Supplementary Videos 7**–**10**). At E12.5 in the developing diaphragm of control embryos, few TUNEL$^+$ apoptotic cells were present (**Fig. 6a**,**c**–**e** and **Supplementary Video 7**) and nearly all muscle progenitors were actively proliferating (**Fig. 6i**,**k**–**m** and **Supplementary Video 9**). In contrast, in mutant embryos, there was a marked increase in the number of apoptotic cells, many of which were present in regions that were abnormally devoid of muscle and consistently give rise to hernias (**Fig. 6b**,**f**–**h** and **Supplementary Video 8**). In addition, there was a profound decrease in the number of ethynyl deoxyuridine (EdU)-positive proliferative cells (**Fig. 6j**,**n**–**p** and **Supplementary Video 10**). Similar to in the heart[43,44], we found that loss of *Gata4* led to decreased levels of the cell cycle regulators cyclin D2 and Cdk4 in PPF cells (**Supplementary Fig. 3**). In culture, isolated *Gata4*-null PPF fibroblasts proliferated at less than half the rate of wild-type fibroblasts (**Supplementary Fig. 4a**). Moreover, when diaphragm myogenic cells were cultured with PPF cells, *Gata4*-null fibroblasts (as compared with wild-type fibroblasts) failed to support the growth of myogenic cells (**Supplementary Fig. 4b**,**c**).

In mutant diaphragms, the number of muscle progenitors is greatly reduced by increased cell death and decreased proliferation, but how do localized amuscular regions develop? In control *Prx1-cre*$^{Tg/+}$; *Gata4*$^{fl/+}$; *Rosa26*$^{mTmG/+}$ embryos, muscle progenitors migrated into and developed completely surrounded by GFP$^+$ PPF cells (**Fig. 6a**,**i** and **Supplementary Videos 7** and **9**). As PPF cells expanded, they carried with them the proliferating and differentiating myogenic cells. In contrast, in *Prx1-cre*$^{Tg/+}$; *Gata4*$^{\Delta/fl}$; *Rosa26*$^{mTmG/+}$ mutants, at E12.5, myogenic cells were largely excluded from GFP$^+$Gata4$^-$ regions (**Fig. 6b**,**j** and **Supplementary Videos 8** and **10**). These localized amuscular regions likely result from the mosaic deletion of one *Gata4* allele by the *Prx1-cre* transgene, which does not efficiently recombine in all PPF cells at E11.5–E12.5 (**Supplementary Fig. 2d**–**i**; the other *Gata4* allele is deleted in the germ line); muscle was excluded from the PPF regions where *Gata4* had been deleted during this early time interval. Only during this early timeframe were myogenic cells sensitive to *Gata4* loss, as deletion of *Gata4* via *Tcf4*^{cre} (ref. 29), which causes recombination in PPF-derived fibroblasts primarily after E12.5, did not result in hernias (n = 16/16; data not shown). Taken together, these data indicate that early mosaic deletion of *Gata4* in PPF cells leads to the increased

apoptosis and decreased proliferation of muscle progenitors and to the development of localized amuscular regions, which ultimately allow herniation (**Fig. 7**).

DISCUSSION

Our study establishes that the PPFs and muscle connective tissue fibroblasts, although previously underappreciated, are critical for the development of the diaphragm and CDH. Not only do PPF cells give rise to the muscle connective tissue and central tendon of the diaphragm, but the connective tissue fibroblasts also control the morphogenesis of the diaphragm's muscle. Our finding that the connective tissue regulates muscle development has precedence, as muscle connective tissue fibroblasts regulate the pattern of limb muscles[28] and the fiber type of limb and diaphragm muscles[29]. To our knowledge, our finding that the active, apparently collective cell migration of connective tissue fibroblasts across the liver's surface controls the expansion of muscle progenitors and overall diaphragm morphogenesis is completely new.

We also definitively demonstrate that defects in the muscle connective tissue fibroblast component of the PPFs are a cellular source of CDH and that *Gata4* null mutations in these cells cause CDH. Surprisingly, we show that hernias do not result from defects in PPF cell migration and the formation of holes in the diaphragm. Instead, PPF deletion of *Gata4* leads to the development of localized amuscular regions through which the growing liver and intestines herniate. In humans, such hernias with connective tissue surrounding the herniated tissue are classified as 'sac hernias' (ref. 6), and we hypothesize that many hernias are covered by connective tissue early in development. Mechanistically, CDH arises when thinner and more compliant amuscular regions develop within the thicker and stiffer muscularized diaphragm and allow herniation. Development of amuscular regions in mutants results from a marked decrease in cell proliferation, an increase in cell death and, most notably, the localized exclusion of myogenic cells from regions with early PPF deletion of *Gata4* and downregulation of HGF expression by muscle connective tissue fibroblasts. Thus, we elucidate how defects in the muscle connective tissue are a potent source of CDH. CDH has been associated with over 50 candidate genes, and several alternative mechanisms of CDH have been described recently[45,46]. An important area of future research will be to determine whether CDH is of heterogeneous origin or if any cellular or molecular defect is common in its etiology.

Our data suggest a new genetic hypothesis for the origin of CDH. Our finding that CDH derives from localized, weaker amuscular regions that develop specifically where *Gata4* has been mutated early in muscle connective tissue fibroblasts suggests that somatic mosaic mutations in fibroblasts may be a genetic feature of some patients with CDH. A potential role for somatic mosaicism in CDH has previously been suggested by the largely discordant occurrence of CDH in monozygotic twins[47], including twins with an 8p23.1 deletion[48], and the finding of genetic mosaicism in patients with CDH[49,50]. Our hypothesis that CDH can arise from somatic mosaic mutations may explain the notable incomplete penetrance and variable expressivity of many CDH-associated CNVs and genetic mutations (particularly in *GATA4*)[11–13,48]. Interestingly, *GATA4* haploinsufficiency in humans and a 70% reduction in *Gata4* expression in mice lead to heart defects with nearly complete penetrance[12,48,51]. In contrast, *GATA4* haploinsufficiency in humans is incompletely penetrant for CDH[12,48], and mice with heterozygous loss of *Gata4* either do not develop CDH (in our data) or do so with low penetrance[16,52]. In addition, for patients with CDH with shared *GATA4* missense mutations[13] or intronic variants[11], the location and severity of hernias are highly variable. Our data suggest the hypothesis that loss of one *GATA4* allele confers susceptibility but is not sufficient to cause CDH; development of CDH requires somatic loss of the second allele in a subset of the connective tissue fibroblasts early during diaphragm morphogenesis. When and where this second allele is deleted determines the size and location of the amuscular region and hernia (CDH expressivity). In humans, somatic mosaicism for *GATA4* mutations and 8p23.1 polymorphisms are well documented[53–56]. Alternatively, the second somatic mosaic, CDH-causative mutation might not involve loss of the second *GATA4* allele but perhaps another CDH-associated gene (resulting in non-allelic non-complementation); multiple CDH-associated genes are strongly expressed in PPF cells, including *Zfpm2* (ref. 19) and *Nr2f2* (ref. 18), which are known to genetically interact with *Gata4*. Thus, the genetic architecture underlying CDH may be complex.

In summary, although muscle connective tissue has often been relegated to a role supporting muscle structure and function, we demonstrate that muscle connective tissue fibroblasts dynamically control diaphragm morphogenesis and that their interactions with muscle progenitors critically regulate the development of the diaphragm's muscle and are a source of CDH. The role of mosaicism in human disease has received increasing attention in recent years[57]. Here we show in mice that mosaic mutations in muscle connective tissue have profound cellular and biomechanical consequences and lead to hernias. We hypothesize that early somatic mosaic mutations might be critical for the etiology of CDH in humans, and this hypothesis will be tested in future experiments.

METHODS

Methods and any associated references are available in the online version of the paper.

Note: Any Supplementary Information and Source Data files are available in the online version of the paper.

ACKNOWLEDGMENTS

We thank C. Rodesch at the University of Utah Imaging Core for help with microscopy, S. Merchant for help with microCT imaging, Y. Wan and C. Hansen for Fluorender analysis, M. Hockin and M.R. Capecchi for Cre protein, and M. Colasanto, N. Elde, L.B. Jorde, A. Keefe, A. Letsou, L.C. Murtaugh and C.J. Tabin for critical comments on the manuscript. A.J.M. was supported by a University of Utah Graduate Fellowship, FEBio analysis is supported by US National Institutes of Health (NIH) grant R01GM083925 to J.A.W. and G.A. Ateshian, and Fluorender analysis is supported by US NIH grant R01GM098151 to C. Hansen. This research was supported by US NIH grant R01HD053728 and March of Dimes grant FY12-405 to G.K.

AUTHOR CONTRIBUTIONS

A.J.M. conducted experiments, analyzed data and wrote the manuscript. Z.D.F. conducted two-photon experiments. B.J.E. and J.A.W. contributed finite element model analysis. J.A.L. managed the mouse colony. G.K. conducted experiments, analyzed data and wrote the manuscript.

COMPETING FINANCIAL INTERESTS

The authors declare no competing financial interests.

1. Perry, S.F., Similowski, T., Klein, W. & Codd, J.R. The evolutionary origin of the mammalian diaphragm. *Respir. Physiol. Neurobiol.* **171**, 1–16 (2010).
2. Campbell, E.J.M., Agostoni, E. & Newsom Davis, J. *The Respiratory Muscles: Mechanics and Neural Control* (Lloyd-Luke, 1970).
3. Merrell, A.J. & Kardon, G. Development of the diaphragm—a skeletal muscle essential for mammalian respiration. *FEBS J.* **280**, 4026–4035 (2013).
4. Raval, M.V., Wang, X., Reynolds, M. & Fischer, A.C. Costs of congenital diaphragmatic hernia repair in the United States—extracorporeal membrane oxygenation foots the bill. *J. Pediatr. Surg.* **46**, 617–624 (2011).

5. Torfs, C.P., Curry, C.J., Bateson, T.F. & Honore, L.H. A population-based study of congenital diaphragmatic hernia. *Teratology* **46**, 555–565 (1992).
6. Pober, B.R. Overview of epidemiology, genetics, birth defects, and chromosome abnormalities associated with CDH. *Am. J. Med. Genet. C. Semin. Med. Genet.* **145C**, 158–171 (2007).
7. Pober, B.R. *et al.* Infants with Bochdalek diaphragmatic hernia: sibling precurrence and monozygotic twin discordance in a hospital-based malformation surveillance program. *Am. J. Med. Genet. A.* **138A**, 81–88 (2005).
8. Holder, A.M. *et al.* Genetic factors in congenital diaphragmatic hernia. *Am. J. Hum. Genet.* **80**, 825–845 (2007).
9. Veenma, D.C., de Klein, A. & Tibboel, D. Developmental and genetic aspects of congenital diaphragmatic hernia. *Pediatr. Pulmonol.* **47**, 534–545 (2012).
10. Russell, M.K. *et al.* Congenital diaphragmatic hernia candidate genes derived from embryonic transcriptomes. *Proc. Natl. Acad. Sci. USA* **109**, 2978–2983 (2012).
11. Arrington, C.B. *et al.* A family-based paradigm to identify candidate chromosomal regions for isolated congenital diaphragmatic hernia. *Am. J. Med. Genet. A.* **158A**, 3137–3147 (2012).
12. Longoni, M. *et al.* Congenital diaphragmatic hernia interval on chromosome 8p23.1 characterized by genetics and protein interaction networks. *Am. J. Med. Genet. A.* **158A**, 3148–3158 (2012).
13. Yu, L. *et al.* Variants in *GATA4* are a rare cause of familial and sporadic congenital diaphragmatic hernia. *Hum. Genet.* **132**, 285–292 (2013).
14. Kuo, C.T. *et al.* GATA4 transcription factor is required for ventral morphogenesis and heart tube formation. *Genes Dev.* **11**, 1048–1060 (1997).
15. Molkentin, J.D., Lin, Q., Duncan, S.A. & Olson, E.N. Requirement of the transcription factor GATA4 for heart tube formation and ventral morphogenesis. *Genes Dev.* **11**, 1061–1072 (1997).
16. Jay, P.Y. *et al.* Impaired mesenchymal cell function in *Gata4* mutant mice leads to diaphragmatic hernias and primary lung defects. *Dev. Biol.* **301**, 602–614 (2007).
17. Mendelsohn, C. *et al.* Function of the retinoic acid receptors (RARs) during development (II). Multiple abnormalities at various stages of organogenesis in RAR double mutants. *Development* **120**, 2749–2771 (1994).
18. You, L.R. *et al.* Mouse lacking COUP-TFII as an animal model of Bochdalek-type congenital diaphragmatic hernia. *Proc. Natl. Acad. Sci. USA* **102**, 16351–16356 (2005).
19. Ackerman, K.G. *et al.* Fog2 is required for normal diaphragm and lung development in mice and humans. *PLoS Genet.* **1**, 58–65 (2005).
20. Coles, G.L. & Ackerman, K.G. Kif7 is required for the patterning and differentiation of the diaphragm in a model of syndromic congenital diaphragmatic hernia. *Proc. Natl. Acad. Sci. USA* **110**, E1898–E1905 (2013).
21. Allan, D.W. & Greer, J.J. Embryogenesis of the phrenic nerve and diaphragm in the fetal rat. *J. Comp. Neurol.* **382**, 459–468 (1997).
22. Babiuk, R.P., Zhang, W., Clugston, R., Allan, D.W. & Greer, J.J. Embryological origins and development of the rat diaphragm. *J. Comp. Neurol.* **455**, 477–487 (2003).
23. Dietrich, S. *et al.* The role of SF/HGF and c-Met in the development of skeletal muscle. *Development* **126**, 1621–1629 (1999).
24. Greer, J.J. *et al.* Structure of the primordial diaphragm and defects associated with nitrofen-induced CDH. *J. Appl. Physiol.* **89**, 2123–2129 (2000).
25. Ackerman, K.G. & Greer, J.J. Development of the diaphragm and genetic mouse models of diaphragmatic defects. *Am. J. Med. Genet. C. Semin. Med. Genet.* **145C**, 109–116 (2007).
26. Logan, M. *et al.* Expression of Cre recombinase in the developing mouse limb bud driven by a *Prx1* enhancer. *Genesis* **33**, 77–80 (2002).
27. Soriano, P. Generalized *lacZ* expression with the ROSA26 Cre reporter strain. *Nat. Genet.* **21**, 70–71 (1999).
28. Kardon, G., Harfe, B.D. & Tabin, C.J.A. Tcf4-positive mesodermal population provides a prepattern for vertebrate limb muscle patterning. *Dev. Cell* **5**, 937–944 (2003).
29. Mathew, S.J. *et al.* Connective tissue fibroblasts and Tcf4 regulate myogenesis. *Development* **138**, 371–384 (2011).
30. Clugston, R.D., Zhang, W. & Greer, J.J. Gene expression in the developing diaphragm: significance for congenital diaphragmatic hernia. *Am. J. Physiol. Lung Cell. Mol. Physiol.* **294**, L665–L675 (2008).
31. Engleka, K.A. *et al.* Insertion of Cre into the *Pax3* locus creates a new allele of *Splotch* and identifies unexpected *Pax3* derivatives. *Dev. Biol.* **280**, 396–406 (2005).
32. Vogan, K.J., Epstein, D.J., Trasler, D.G. & Gros, P. The splotch-delayed (*Sp^d*) mouse mutant carries a point mutation within the paired box of the *Pax-3* gene. *Genomics* **17**, 364–369 (1993).
33. Watt, A.J., Battle, M.A., Li, J. & Duncan, S.A. GATA4 is essential for formation of the proepicardium and regulates cardiogenesis. *Proc. Natl. Acad. Sci. USA* **101**, 12573–12578 (2004).
34. Ackerman, K.G. *et al.* Congenital diaphragmatic defects: proposal for a new classification based on observations in 234 patients. *Pediatr. Dev. Pathol.* **15**, 265–274 (2012).
35. Clugston, R.D. & Greer, J.J. Diaphragm development and congenital diaphragmatic hernia. *Semin. Pediatr. Surg.* **16**, 94–100 (2007).
36. Maas, S.A., Ellis, B.J., Ateshian, G.A. & Weiss, J.A. FEBio: finite elements for biomechanics. *J. Biomech. Eng.* **134**, 011005 (2012).
37. Strumpf, R.K., Humphrey, J.D. & Yin, F.C. Biaxial mechanical properties of passive and tetanized canine diaphragm. *Am. J. Physiol.* **265**, H469–H475 (1993).
38. Keijzer, R., Liu, J., Deimling, J., Tibboel, D. & Post, M. Dual-hit hypothesis explains pulmonary hypoplasia in the nitrofen model of congenital diaphragmatic hernia. *Am. J. Pathol.* **156**, 1299–1306 (2000).
39. Ackerman, K.G. *et al. Gata4* is necessary for normal pulmonary lobar development. *Am. J. Respir. Cell Mol. Biol.* **36**, 391–397 (2007).
40. Bladt, F., Riethmacher, D., Isenmann, S., Aguzzi, A. & Birchmeier, C. Essential role for the c-Met receptor in the migration of myogenic precursor cells into the limb bud. *Nature* **376**, 768–771 (1995).
41. Maina, F. *et al.* Uncoupling of Grb2 from the Met receptor *in vivo* reveals complex roles in muscle development. *Cell* **87**, 531–542 (1996).
42. Nakamura, K., Hongo, A., Kodama, J. & Hiramatsu, Y. The role of hepatocyte growth factor activator inhibitor (HAI)-1 and HAI-2 in endometrial cancer. *Int. J. Cancer* **128**, 2613–2624 (2011).
43. Rojas, A. *et al.* GATA4 is a direct transcriptional activator of cyclin D2 and Cdk4 and is required for cardiomyocyte proliferation in anterior heart field–derived myocardium. *Mol. Cell. Biol.* **28**, 5420–5431 (2008).
44. Yamak, A. *et al.* Cyclin D2 rescues size and function of GATA4 haplo-insufficient hearts. *Am. J. Physiol. Heart Circ. Physiol.* **303**, H1057–H1066 (2012).
45. Domyan, E.T. *et al.* Roundabout receptors are critical for foregut separation from the body wall. *Dev. Cell* **24**, 52–63 (2013).
46. Zhang, B. *et al.* Heparan sulfate deficiency disrupts developmental angiogenesis and causes congenital diaphragmatic hernia. *J. Clin. Invest.* **124**, 209–221 (2014).
47. Veenma, D. *et al.* Copy number detection in discordant monozygotic twins of congenital diaphragmatic hernia (CDH) and esophageal atresia (EA) cohorts. *Eur. J. Hum. Genet.* **20**, 298–304 (2012).
48. Wat, M.J. *et al.* Chromosome 8p23.1 deletions as a cause of complex congenital heart defects and diaphragmatic hernia. *Am. J. Med. Genet. A.* **149A**, 1661–1677 (2009).
49. Kantarci, S. *et al.* Characterization of the chromosome 1q41q42.12 region, and the candidate gene *DISP1*, in patients with CDH. *Am. J. Med. Genet. A.* **152A**, 2493–2504 (2010).
50. Veenma, D. *et al.* Comparable low-level mosaicism in affected and non affected tissue of a complex CDH patient. *PLoS ONE* **5**, e15348 (2010).
51. Pu, W.T., Ishiwata, T., Juraszek, A.L., Ma, Q. & Izumo, S. GATA4 is a dosage-sensitive regulator of cardiac morphogenesis. *Dev. Biol.* **275**, 235–244 (2004).
52. Wat, M.J. *et al.* Mouse model reveals the role of SOX7 in the development of congenital diaphragmatic hernia associated with recurrent deletions of 8p23.1. *Hum. Mol. Genet.* **21**, 4115–4125 (2012).
53. Bosch, N. *et al.* Nucleotide, cytogenetic and expression impact of the human chromosome 8p23.1 inversion polymorphism. *PLoS ONE* **4**, e8269 (2009).
54. Giglio, S. *et al.* Olfactory receptor-gene clusters, genomic-inversion polymorphisms, and common chromosome rearrangements. *Am. J. Hum. Genet.* **68**, 874–883 (2001).
55. Reamon-Buettner, S.M. & Borlak, J. GATA4 zinc finger mutations as a molecular rationale for septation defects of the human heart. *J. Med. Genet.* **42**, e32 (2005).
56. Reamon-Buettner, S.M., Cho, S.H. & Borlak, J. Mutations in the 3′-untranslated region of *GATA4* as molecular hotspots for congenital heart disease (CHD). *BMC Med. Genet.* **8**, 38 (2007).
57. Biesecker, L.G. & Spinner, N.B. A genomic view of mosaicism and human disease. *Nat. Rev. Genet.* **14**, 307–320 (2013).

ONLINE METHODS

Mice. All mice have been previously published. We used *Prx1-cre* (ref. 26), *Pax3*^{cre} (ref. 31) and *Hprt-cre* (ref. 58) Cre alleles, *Rosa26*^{LacZ} (ref. 27) and *Rosa26*^{mTmG} (ref. 59) Cre-responsive reporter alleles, and *Pax3*^{SpD} (ref. 32) and *Gata4*^{fl} (ref. 33) mutant alleles. *Gata4*$^{\Delta/+}$ mice were generated by breeding *Gata4*^{fl} mice to *Hprt-cre* mice. Mice were backcrossed onto the C57BL6/J background. No statistical method was used to predetermine sample size, all mice were included and the experiments were not randomized. Mouse experiments were performed in accordance with protocols approved by the Institutional Animal Care and Use Committee at the University of Utah.

Immunofluorescence, β-galactosidase staining and microscopy. For section immunofluorescence, embryos were fixed, embedded, cryosectioned and immunostained as described previously[29]. EdU (Life Technologies) was detected according to the manufacturer's directions. For TUNEL (terminal deoxynucleotidyl transferase dUTP nick end labeling) staining, embryos were incubated in TUNEL reaction solution at 37 °C for 1 h. For whole-mount immunofluorescence, embryos were fixed for 24 h in 4% paraformaldehyde, dissected, incubated for 24 h in Dent's bleach (1:2 30% H_2O_2:Dent's fix) and stored in Dent's fix (1:4 DMSO:methanol) for at least 5 d. Embryos were washed in PBS, blocked for 1 h in 5% serum and 20% DMSO, incubated in primary antibody at room temperature for 48 h, washed in PBS, incubated in secondary antibody for 48 h, washed in PBS and subjected to the EdU reaction for 1 h. Diaphragms were cleared in BABB (33% benzyl alcohol, 66% benzyl benzoate). Alkaline phosphatase–conjugated mouse IgG1 antibody to My32 was incubated for 48 h and detected with 250 μg/ml NBT and 125 μg/ml BCIP (Sigma) in NTMT.

Cultured cells were fixed for 20 min in 4% paraformaldehyde, blocked in 5% serum in PBS with 0.1% Triton X-100 for 1 h, incubated in primary antibody at 4 °C overnight, washed with PBS and incubated for 2 h in secondary antibody. Following antibody staining, EdU was detected as described above. Cells were incubated in 0.4 μg/ml Hoechst for 5 min and mounted with Fluoromount-G. Antibodies are listed in **Supplementary Table 1**.

For whole-mount β-galactosidase staining, embryos were fixed for 1.5 h in 4% paraformaldehyde and 2 mM $MgCl_2$. Diaphragms were dissected, washed in PBS and rinse buffer (100 mM sodium phosphate, 2 mM $MgCl_2$, 0.01% sodium deoxycholate and 0.02% IGEPAL) and stained for 16 h at 37 °C in X-gal staining solution (5 mM potassium ferricyanide, 5 mM potassium ferrocyanide and 1 mg/ml X-gal).

Fluorescent images were taken on a Nikon A1 confocal microscope. Optical stacks of whole mounts were rendered using FluoRender[60]. β-galactosidase–stained embryos were imaged with a Qimaging camera. All analyses were performed with blinding.

Cell culture. Fibroblasts were isolated from E15.5 *Gata4*$^{fl/fl}$; *Rosa26*$^{mTmG/+}$ or *Rosa26*$^{mTmG/+}$ diaphragms, cultured and expanded for 3 weeks. We added 4 μM TAT-Cre (M. Hockin and M.R. Capecchi, University of Utah) to induce recombination. EdU was given 4 h before fixation and immunofluorescence. For co-cultures, fibroblasts and myoblasts were isolated from E15.5 *Prx1-cre*$^{Tg/+}$; *Gata4*$^{\Delta/fl}$; *Rosa26*$^{mTmG/+}$ or *Prx1-cre*$^{+/+}$; *Gata4*$^{\Delta/fl}$; *Rosa26*$^{mTmG/+}$ diaphragms, cultured for 2 d and given EdU 1 h before fixation and immunofluorescence. Analysis of statistical significance was performed by two-tailed Student's *t* test.

Diaphragm explants. E12.5 *Prx1-cre*$^{Tg/+}$; *Rosa26*$^{mTmG/+}$ mice were sacrificed and trimmed to only include the diaphragm with attached ribs, hind limbs and liver. Explanted diaphragms were cultured for 2–6 h in 100% horse serum at 37 °C in the presence of 5% CO_2. Explants were imaged on a Bruker (Prairie) two-photon microscope, and four-dimensional data sets were rendered and visualized using FluoRender[60]. Individual cells were tracked using FluoRender.

Modeling. To gain insights into the biomechanics of herniation, we used finite element modeling, a computational method for assembling the response of a complex system from the individual contributions of discrete elements[36]. The finite element model of hernia development was based on an E16.5 *Prx1-cre*$^{Tg/+}$; *Gata4*$^{\Delta/fl}$ herniated mouse diaphragm. The geometry of the diaphragm was based on surfaces created from segmenting microscopy images. Surfaces were discretized with quadratic-tetrahedral elements, and the adequacy of the spatial discretization was confirmed with a mesh convergence study. Meshes were created with ANSA software (BETA CAE Systems USA) and analyzed with FEBio[36]. For the simulations, the rib cage surrounding the diaphragm was rigidly constrained in the model (kept immobile), while a uniform pressure of 380 Pa was applied to simulate the pressure applied by the liver. The pressure was chosen so that the bulge height of the muscle region predicted by the model matched the height measured in the experiment. The muscle was represented by an isotropic hyperelastic Veronda-Westmann constitutive equation[61] with coefficients $C_1 = 2.1$ MPa, $C_2 = 0.1$ and $K = 10$ based on published data[37]. The connective tissue of the hernia was represented with an isotropic hyperelastic Mooney-Rivlin constitutive equation[62] using either the coefficients $C_1 = 0.003$ MPa and $K = 1$ or $C_1 = 0.01$ MPa and $K = 10$.

MicroCT analysis of lungs. Embryos were fixed in 4% paraformaldehyde in PBS overnight. Lungs were removed, pretreated with 25% Lugol's solution for 1 h and then soaked in PBS for 1 h before imaging. CT images consisting of 360 degrees and 600 projections were acquired using an Inveon trimodality PET/SPECT/CT scanner (Siemens Preclinical Solutions). The exposure time was 2.9 s with detector settings at 80 kVp and 150 μA. Data were reconstructed onto a 1,792 × 1,792 × 2,688 image matrix using the COBRA software package (Exxim Computing Corporation,). The effective image voxel size was 33.6 μm isotropic. Reconstructed images were analyzed using Osirix software.

58. Tang, S.H., Silva, F.J., Tsark, W.M. & Mann, J.R.A. Cre/*lox*P-deleter transgenic line in mouse strain 129S1/SvImJ. *Genesis* **32**, 199–202 (2002).
59. Muzumdar, M.D., Tasic, B., Miyamichi, K., Li, L. & Luo, L. A global double-fluorescent Cre reporter mouse. *Genesis* **45**, 593–605 (2007).
60. Wan, Y., Otsuna, H., Chien, C.B. & Hansen, C. An interactive visualization tool for multi-channel confocal microscopy data in neurobiology research. *IEEE Trans. Vis. Comput. Graph.* **15**, 1489–1496 (2009).
61. Veronda, D.R. & Westmann, R.A. Mechanical characterization of skin-finite deformations. *J. Biomech.* **3**, 111–124 (1970).
62. Mooney, M. A theory of large elastic deformation. *J. Appl. Phys.* **11**, 582–592 (1940).